Wave Envelope and Finite Element Approximations for Turbofan Noise Radiation in Flight

A. V. Parrett*
General Motors Proving Ground, Milford, Michigan
and
W. Eversman†
University of Missouri-Rolla, Missouri

The problem of acoustic radiation from turbofan engine inlets in flow has not lent itself fully to analysis by numerical means because of the large domains and high frequencies involved. The current work has extended the use of finite elements and wave envelope elements, elements that simulate decay and wavelike behavior in their interpolation functions, from the no-flow case in which they have proven, to cases incorporating mean flow. By employing an irrotational mean flow assumption, the acoustics problem has been posed in an axisymmetric formulation in terms of acoustic velocity potential, thus minimizing computer solution storage requirements. The results obtained from the numerical procedures agree well with known analytical solutions, static experimental jet engine inflow data, and flight test results.

Nomenclature

a_i^+, a_i^- = incident and reflected modal amplitudes, respectively
c = nondimensional speed of sound in flow
e_i^+, e_i^- = positive and negative uniform duct eigenfunctions, respectively
m = spinning mode number
N_i = interpolation function
p = pressure
t = time
u = axial component of local Mach number
U = Mach number
v = radial component of local Mach number
v = acoustic velocity
V = velocity
x = axial coordinate
γ = ratio of specific heats
ϵ = penalty parameter
η, ξ = local finite element coordinates
κ, λ = local and axial wave numbers, respectively
μ = uniform duct eigenvalue
ρ = density
ϕ = velocity potential, trial function
$\Phi(\Omega)$ = trial function space
Φ = full nondimensional velocity potential
ψ = test function
$\Psi(\Omega)$ = test function space
ω = harmonic frequency

Superscripts

$( )'$ = nondimensional quantity, derivative (see text)
e = quantity defined inside a finite element

Subscripts

0 = mean flow quantity
i = nodal value, summation index (see text)

Introduction

THE study of fan noise has become increasingly important with the widespread use in civil aircraft of high-bypass-ratio turbofan engines. Although the bypass design has the beneficial effect of reducing jet noise at the rear of the engine by lowering jet velocity, significant forward sound propagation of fan noise is of concern, particularly on landing approaches.

The acoustical analysis for the forward propagating noise involves the noise generation by the fan, the propagation inside the inlet cowling, and the radiation from the inlet to the far field, and there has been much work to date in the former two areas in relation to duct acoustics.[1-3]

The radiation problem poses some severe difficulties because of the effectively infinite domain involved and the presence of flow. The use of finite element (FE) methods was precluded because of storage limitations until the infinite domain could be modeled. Horowitz, Sigman, and Zinn used a hybrid FE-integral technique for no-flow problems,[4] then extended this to cases involving flow.[5] The technique uses an iterative procedure between an inner region FE formulation and a boundary element representation in the far field, and the solution times are high.[5] The present work differs from this approach by modeling the far field using wave envelope elements, which simulate wavelike behavior in their interpolation functions. The method is an extension of the no-flow work by Astley and Eversman[6] and the flow studies of Astley,[7] to include realistic flow cases and inlet acoustic effects. The use of wave envelope elements relies on the assumption that at some distance from the inlet the sound field approximates that produced by a point source and makes feasible a numerical solution of the acoustical radiation problem by drastically reducing storage requirements. The inner region is modeled using finite elements, and inter-element compatibility at the interface is ensured by the wave envelope element interpolation functions used, so that no solution iteration is required. This results in a considerable time saving over the hybrid FE-integral approach.

In the interests of computational efficiency, an axisymmetric problem formulation based on acoustic velocity

Presented as Paper 84-2333 at the AIAA/NASA Ninth Aeroacoustics Conference, Williamsburg, VA, Oct. 15-17, 1984; received Nov. 16, 1984; revision received Sept. 20, 1985.

*Senior Project Engineer, Noise and Vibration Laboratory. Member AIAA.
†Curators' Professor, Mechanical and Aerospace Engineering Department. Associate Fellow AIAA.

potential (hence the assumption of an ideal fluid, and also that of an irrotational flowfield, both in the mean flow and acoustic perturbations) has been employed. This approach follows one used successfully by Tag and Lumsdaine,[3] among others. The external flow is assumed to be uniform, steady, of low subsonic Mach number, and parallel to the axis of symmetry. The low Mach number and ideal fluid assumptions are valid for situations such as landing approaches.

The inlet is modeled as a duct with the fan plane at a section of locally uniform area with uniform flow, and the acoustic pressure field at the fan plane is modeled by a combination of incident and reflected (positive and negative) uniform duct eigenfunctions. The nacelle is regarded as impervious to flow, and in the far field a Sommerfeld radiation condition is applied on a boundary at a large but finite distance from the inlet.

To avoid modeling the rear of the engine and to decrease the size of the computational domain, an artificial boundary is implied (see Fig. 1). This may be thought of as a baffle that would admit flow-through yet interfere with the forward radiated acoustic field to as small an extent as possible.

Equations of Motion

It is assumed that the medium is inviscid and non-heat conducting with constant specific heats, and that all processes are isentropic.

Under these assumptions, the governing equations for the problem may be written in nondimensional form as

Mass conservation:

$$\frac{\partial \rho'}{\partial t'} + \nabla \cdot (\rho' V') = 0 \tag{1}$$

Momentum conservation:

$$\frac{\partial V'}{\partial t'} + (V' \cdot \nabla) V' = \frac{-1}{\rho'} \nabla p' \tag{2}$$

Equation of state:

$$p' = (1/\gamma)\rho'^{\gamma} \tag{3}$$

The nondimensional speed of sound can be written as

$$c'^2 = \gamma p'/\rho' = \rho'^{\gamma - 1} \tag{4}$$

The flowfield is assumed to be irrotational, so

$$V' = \nabla \Phi' \tag{5}$$

If it is assumed that the reference conditions are taken to be stagnation conditions ($|V'| = 0$, $c' = 1$, $\partial/\partial t = 0$), the momentum equation in terms of density and velocity potential may be cast as

$$c'^2 = 1 - (\gamma - 1)\left[\frac{\partial \Phi'}{\partial t} + \frac{1}{2}(\nabla \Phi' \cdot \nabla \Phi')\right]$$

$$= \rho'^{\gamma - 1} \tag{6}$$

The mass conservation equation then becomes

$$\frac{\partial \rho'}{\partial t} + \nabla \cdot (\rho' \nabla \Phi') = 0 \tag{7}$$

Linearized Perturbed Equations

The assumption that the acoustic quantities consist of small perturbations superimposed on a time-invariant flowfield is now made, so that

$$\Phi' = \phi_0 + \phi, \qquad \rho' = \rho_0 + \rho \tag{8}$$

Substitution of Eq. (8) into Eqs. (6) and (7), and linearization of quantities to first order in acoustic perturbations, then yields

$$\rho_0 = \left[1 - \frac{(\gamma - 1)}{2} \nabla \phi_0 \cdot \nabla \phi_0\right]^{1/(\gamma - 1)} \tag{9}$$

$$\rho = -\frac{\rho_0}{c^2}\left[\frac{\partial \phi}{\partial t} + \nabla \phi_0 \cdot \nabla \phi\right] \tag{10}$$

where

$$c^2 = \rho_0^{\gamma - 1} \tag{11}$$

and (the mass conservation equation)

$$\frac{\partial \rho}{\partial t} + \nabla \cdot (\rho_0 \nabla \phi + \rho \nabla \phi_0) = 0 \tag{12}$$

Substitution for ρ_0 and ρ from Eqs. (9) and (10) results in a single equation formulation in terms of the scalar velocity potential. The acoustic pressure is related to the acoustic potential by

$$p = -\frac{\rho_0}{c}\left[\frac{\partial \phi}{\partial t} + \nabla \phi_0 \cdot \nabla \phi\right] \tag{13}$$

Inlet Flow Problem

Under the assumption of low mean flow Mach numbers, the mean flow density is approximately constant; thus the flow problem may be posed (with reference to Fig. 1) as

$$\nabla^2 \phi_0 = 0 \text{ in } \Omega \tag{14a}$$

$$\nabla \phi_0 \cdot \boldsymbol{n} = -cU_1 \text{ on } \Gamma_1 \tag{14b}$$

$$\phi_0 = cUx \text{ on } \Gamma_3, \Gamma_4 \tag{14c}$$

$$\nabla \phi_0 \cdot \boldsymbol{n} = 0 \ \Gamma_5 \tag{14d}$$

In Fig. 1, the curves Γ in the (x,r) plane correspond to surfaces C in axisymmetric 3 space.

The axis of symmetry Γ_2 is not a physical boundary in 3 space. As a consequence, in the axisymmetric integral formulation of the problem used, the boundary integrals on the axis ($r = 0$) are always zero, therefore no boundary condition need be specified.

The far-field boundary Γ_3 of Fig. 1 is circular (spherical in 3 space). It is assumed that this boundary is located at a distance far from the inlet so that the flow effects due to the presence of the inlet are negligible.

The curve Γ_4 in Fig. 1 represents a pseudoboundary that is not present in physical problems but is desirable for obtain-

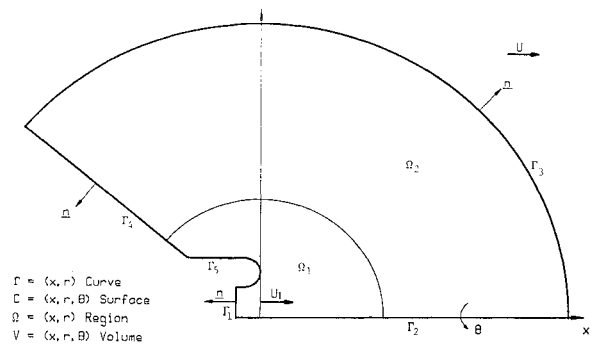

Fig. 1 Inlet geometry.

ing solutions by numerical method, since by reducing the domain size it diminishes computational storage requirements. The boundary would correspond physically to a porous baffle that would admit flow through and affect the acoustic field to as small an extent as possible. The angle the baffle makes with the axis of symmetry must be a compromise between one near 90 deg, which would tend to produce standing wave interference in the acoustic field, and one near 180 deg, which would not model the rear of the engine properly due to the flow effects of the jet exit.

Acoustics Problem with Flow

Consider Eq. (12): from the expression for acoustic density (10), it can be seen that the first term in the divergence contains terms in both the acoustic potential and its gradient. The formulation used here groups both first and second derivative terms, and with the divergence term as shown leads naturally to the implementation of the far-field boundary conditions for the inlet acoustics problem with flow.

To model a classical Sommerfeld radiation condition of an outgoing wave, it is assumed that the boundary Γ_3 of Fig. 1 is far enough from the inlet that the physical situation approximates an acoustic monopole in a uniform flow whose analytical solution is

$$\phi=\frac{1}{R}\exp[i(\omega t-\kappa S)] \tag{15}$$

where

$$S=\frac{1}{(1-U^2)}(-Ux+R) \tag{16}$$

$$R=(x^2+(1-U^2)r^2)^{1/2} \tag{17}$$

$$\kappa=\omega/c \tag{18}$$

Under this assumption the far-field boundary condition may be expressed as

$$(\rho\nabla\phi_0+\rho_0\nabla\phi)\cdot\boldsymbol{n}$$

$$=\rho_0\left(-i\kappa-\frac{(1-U^2)}{R}\right)\frac{1}{R}\begin{Bmatrix}x\\r\end{Bmatrix}\cdot\begin{Bmatrix}n_x\\n_r\end{Bmatrix}\phi \text{ on } \Gamma_3 \tag{19}$$

where n_x, n_r are the components of the normal to the curve in the (x,r) plane. The boundary condition in the far field for the boundary Γ_4 may also be modeled by Eq. (19).

The boundary Γ_1 is taken to be at a locally uniform part of the inlet. To specify the potential there, a duct eigenvalue problem is solved; then the eigenvectors and eigenvalues obtained are used for evaluating terms required for the natural boundary condition implied by a weak formulation of Eq. (12). This matching can be expressed as

$$\phi=\sum_{i=1}^{M}a_i^+e_i^+ + \sum_{i=1}^{M}a_i^-e_i^-$$

where M is the number of terms used in the modal expansion.

The inlet plane boundary condition may then be expressed in a similar manner to Eq. (19) as

$$(\rho\nabla\phi_0+\rho_0\nabla\phi)\cdot\boldsymbol{n}=i\rho_0\Bigg[\sum_{j=1}^{M}((1-U_1^2)\lambda_j^+ +\kappa U_1)a_j^+e_j^+$$

$$+\sum_{j=1}^{M}((1-U_1^2)\lambda_j^- +\kappa U_1)a_j^-e_j^-\Bigg] \text{ on } \Gamma_1$$

The axial wave numbers $\lambda_j^{\pm}$ are obtained from a duct eigenvalue problem, the a^+ are specified, and the a^- are part of the solution.

To give comparisons of computed and analytical results, test cases of vibrating spheres with appropriate analytical solutions[9] are used.

Numerical Solutions

Flow Problem

To solve Laplace's equation with the Neumann and Dirichlet boundary conditions as expressed in Eqs. (14a-d), the following weak problem is posed:

Find $\phi\epsilon\Phi(\Omega)$ such that

$$\frac{1}{c}\int_\Omega\nabla\psi\cdot\nabla\phi+\frac{1}{\epsilon}\int_{\Gamma_4}\psi(\phi-Ux)$$

$$=-\int_{\Gamma_1}\psi U_l+\int_{\Gamma_3}\psi Ui\cdot\boldsymbol{n}\forall\ \psi\epsilon\Psi(\Omega), \text{ and some } \epsilon>0$$

where the quantities are defined in Fig. 1 and Eqs. (14a-d) and $\Phi(\Omega)$ and $\Psi(\Omega)$ are suitable classes of functions whose derivatives are square integrable (H^1) functions. The Dirichlet condition on Γ_4 is implemented above by penalization, where ϵ is a penalty parameter whose value is typically 10^{-20}.

A Galerkin FE approximation is used with eight noded isoparametric quadrilateral elements, and the resultant system of equations solved on a computer. (See Ref. 8 for details of FE methods used in this section.)

Acoustics

In order to formulate a suitable weak problem, first make the assumption that the trial and test functions may be written as

$$\phi=\phi(x,r)\exp[i(\omega t-m\theta)],\quad \psi=\psi(x,r)\exp[-i(\omega t-m\theta)] \tag{20}$$

The test functions ψ are taken to be complex conjugates of the trial functions ϕ consistent with the definition of the inner product of a complex Hilbert space. The weak problem in the (x,r) domain is posed as:

Find $\phi\epsilon\Phi(\Omega)$ such that

$$\int_\Omega[i\omega\psi\rho-\nabla\psi\cdot(\rho\nabla\phi_0+\rho_0\nabla\phi)]$$

$$=-i\int_{\Gamma_1}\rho_0\psi\Bigg[\sum_{j=1}^{M}((1-U_1^2)\lambda_j^+ +\kappa U_1)a_j^+e_j^+$$

$$+\sum_{j=1}^{M}((1-U_1^2)\lambda_j^- +\kappa U_1)a_j^-e_j^-\Bigg]$$

$$-\int_{\Gamma_3+\Gamma_4}\rho_0\psi\left(-i\kappa-\frac{(1-U^2)}{R}\right)\frac{1}{R}\begin{Bmatrix}x\\r\end{Bmatrix}\cdot\begin{Bmatrix}n_x\\n_r\end{Bmatrix}\phi$$

$$\forall\ \psi\epsilon\Phi(\Omega) \tag{21}$$

where

$$[i\omega\psi\rho-\nabla\psi\cdot(\rho\nabla\phi_0+\rho_0\nabla\phi)]$$

$$=\rho_0[(\kappa^2-(m^2/r^2))\psi\phi+i\kappa u(\psi_x\phi+\phi\psi_x)$$

$$+i\kappa v(\psi_r\phi+\phi\psi_r)-(1-u^2)\psi_x\phi_x$$

$$-(1-v^2)\psi_r\phi_r+uv(\psi_x\phi_r+\psi_r\phi_x)] \tag{22}$$

and $\Phi(\Omega)$, $\Psi(\Omega)$ are appropriate complex H^1 function subspaces, and the subscripts denote partial derivatives.

The finite element approximation of this problem differs from that for the flow problem. Observation of Fig. 1 shows

the domain in the (x,r) plane to be divided into two regions. Eight noded isoparameteric quadrilateral elements were again chosen, and in the inner region, Ω_1, the interpolation functions used are the same as those for the flow problem.

The modeling of the outer region is the crux of this problem. For the large (effectively infinite) domain, approximation using conventional finite elements would be too costly in computational time and storage to implement.

Astley and Eversman[6] gave comparisons of infinite element formulations with a wave envelope approach and found the latter to be more suited to the acoustics problem. By assuming that from a sufficiently large distance an inlet approximates a point source, a wave envelope element function of the following form is used

$$f^e = \sum_{i=1}^{n} N_i(\xi,\eta)\frac{R_i}{R}\exp[-ik'(\xi-\xi_i)]f_i^e$$

where R is as defined in Eq. (17), $k'=\kappa\Delta S/2$, ΔS is the difference in the value of S in Eq. (16) between the inner and outer element boundaries, and N_i is a standard FE interpolation function. Element formulations both with and without the decay R_i/R term have been tested (in each case the N_i were the same). The far-field mesh construction is based on the constant phase surfaces of the monopole solution. Wave envelope element boundaries are taken to be lines [in the (x,r) plane] of constant phase and ray paths that correspond to lines through the origin (see, for example, Figs. 3 and 5). This mesh ensures interelement compatibility for interpolation functions both with and without decay terms in the wave envelope element region as well as at the finite element interface. In the programming, the term $\exp[i\kappa(S_j-S_i)]$ may be evaluated very simply, since by construction of the mesh and function it is required that S be linear in ξ. This means that there is only a minimal penalty involved in calculating exponentials for an element matrix over conventional finite element calculations.

Boundary Conditions

1) The Axis: Observation of Eq. (22), the domain integral, shows that for a nonzero value of m, the term

$$\int_\Omega \rho_0\left(\kappa^2-\frac{m^2}{r^2}\right)\psi\phi$$

becomes singular on the axis (the axisymmetric formulation results in a first-order singularity in r under the domain integral). The approximation of the integral numerically by Gauss-Legendre quadrature means that the terms in the integrand are evaluated not at $r=0$ but at some small distance off axis so that they are large but finite. The corresponding components in the resultant matrices associated with the on-axis nodes thus dominate all others. Since the boundary integrals give zero contributions, this results in effectively penalizing the value of the acoustic potential to be zero on the axis when spinning modes are present.

2) The Far Field: The far-field mesh is constructed on the basis of the constant phase surfaces for a harmonic acoustic monopole and is shown in Fig. 1. This choice of mesh simplifies the far-field boundary conditions greatly. The boundary integral on Γ_3 thus becomes

$$\int_{\Gamma_3}\left(-i\kappa-\frac{(1-U^2)}{R}\right)\frac{1}{R}\begin{Bmatrix}x\\r\end{Bmatrix}\cdot\begin{Bmatrix}n_x\\n_r\end{Bmatrix}\phi$$

$$=\int_{\Gamma_3}\left(-i\kappa-\frac{(1-U^2)}{R}\right)\phi$$

As R becomes large, the first term under the integral dominates and the boundary conditions approximates a locally plane wave (a ρc condition).

3) The Baffle: Application of the far-field boundary condition for an acoustic monopole in flow as in the previous section means that on a baffle that corresponds to a segment of a line passing through the origin in the (x,r) plane, the boundary integral vanishes. This approximation is valid in the far-field where the inlet is assumed to be equivalent to a point source, however it has also been assumed for the near field, with the expectation that any errors induced will be localized and not contribute significantly to the forward radiation field.

4) The Inlet: The uniform duct eigenfunction were obtained by solving a numerical eigenvalue problem as in Ref. 10. The accuracy of the resultant eigenvalues indicated whether the FE mesh was fine enough for the radiation problem solution.

The matrix system resulting from the finite element procedure is underdetermined, so equations implying pressure continuity are appended (in the same manner as in Ref. 6) to yield

$$\begin{bmatrix}[D^-] & [B^-]^T\\ [B^-] & [A]\end{bmatrix}\begin{Bmatrix}a^-\\ \phi\end{Bmatrix}=-\begin{bmatrix}[D^+]\\ [B^+]\end{bmatrix}\{a^+\}$$

in which $[A]$ results from Eq. (22),

$$B_{jk}^{\pm}=i\int_{\Gamma_1}\rho_0 N_j((1-U_1^2)\lambda_k^-+\kappa U_1)e_k^{\pm}$$

$$D_{jk}^{\pm}=-i\int_{\Gamma_1}\rho_0 e_j^-((1-U_1^2)\lambda_j^-+\kappa U_1)e_k^{\pm}$$

Computational Aspects

To judge how well the FE solution compared with the analytic solution for a test case, it was decided to use the L^2 norm over the domain. Although convergence in this norm is not a sufficient condition for convergence of the FE solution, it is necessary, and it gives some measure of the accuracy of a solution, when considering such things as the resolution of the mesh in number of finite elements per wavelength. Comparing results on the nodal basis would be tedious, given the number of mesh points involved in a typical problem.

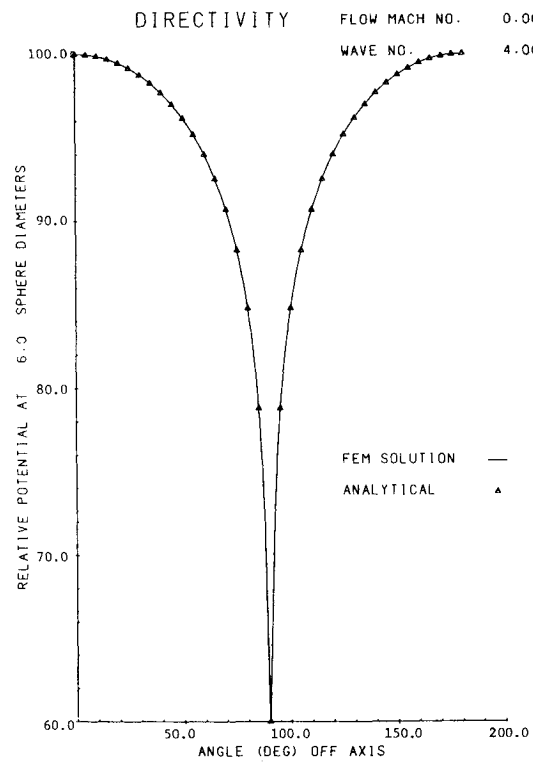

Fig. 2 Potential directivity, juddering sphere, $U=0$, $\kappa=4$.

Because of the large numbers of nodes in such a problem, various time- and space-saving techniques were used in the computations. The system of equations was solved using out-of-core, banded solution methods. An equally appropriate frontal solution technique has also been used and is standard in the production version of the software.

Results and Discussion

Analytical Solutions

1) Flow over a Harmonic Acoustic Monopole: To establish finite element mesh resolution for acoustic wave propagation, a mesh was constructed similar to the inner region of Fig. 3. At the inner radius, a (Dirichlet) monopole boundary condition is applied using penalization (thus avoiding singularity effects at the origin and derivative effects at $r=0.5$ from a pulsating sphere (Neumann) boundary condition). A mesh resolution of five quadratic finite elements per acoustic wavelength was established based on L^2 norm considerations (the error norm was approximately 1% of the solution norm). The introduction of a uniform flow ($U=-0.3$) with appropriately convected mesh did not change the error norm significantly, however small scale (relative to the acoustic wavelength) geometric or reflection effects would require finer mesh resolution for a given degree of accuracy.

2) Flow over a Juddering Sphere: A juddering sphere is one in which the radius remains fixed but the center oscillates along the axis. A unit diameter sphere was modeled (again penalizing the boundary condition) with the oscillation wave number $\kappa=4$. The analytical solution is described in Ref. 9, and in the limit as the radius approaches zero, it approximates a dipole aligned with the axis of symmetry.

Two cases are considered, at Mach numbers 0,0 and -0.2. Wave envelope elements without decay terms in their interpolation functions have been employed, and the finite element-wave envelope element transition radius was established on the basis of L^2 error norm considerations for the no-flow case. The mesh for the flow/acoustics solution is the same as that for the no-flow/acoustics solution with appropriate shift to preserve element size in relation to the acoustic wavelength.

Figures 2 and 3 show the potential directivity and pressure magnitude plots, respectively, for the zero Mach number case. The patterns show typical dipole radiation characteristics, with the positive and negative (with respect to the

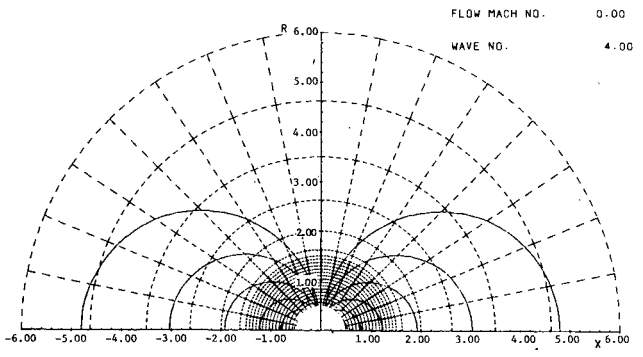

Fig. 3 Pressure magnitude, juddering sphere, $U=0$, $\kappa=4$.

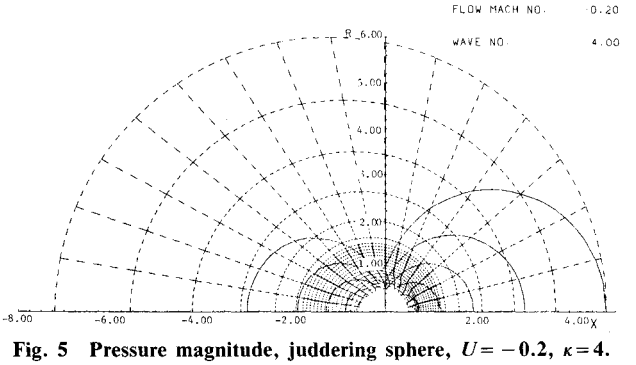

Fig. 5 Pressure magnitude, juddering sphere, $U=-0.2$, $\kappa=4$.

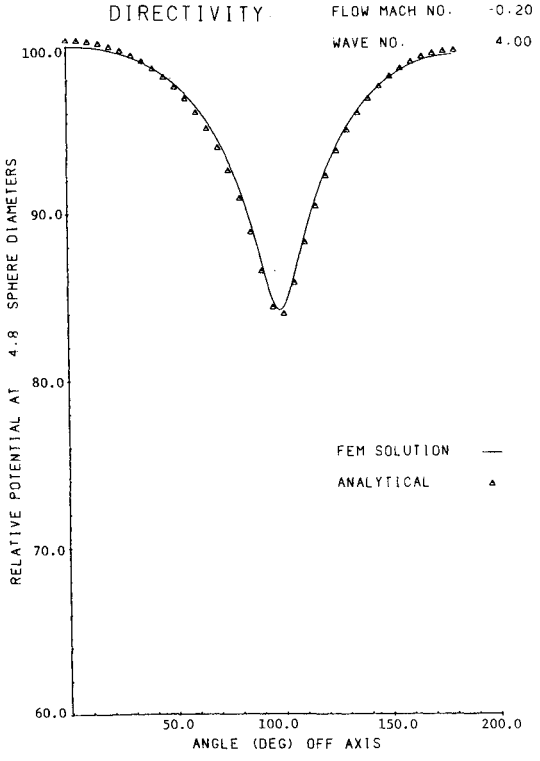

Fig. 4 Potential directivity, juddering sphere, $U=-0.2$, $\kappa=4$.

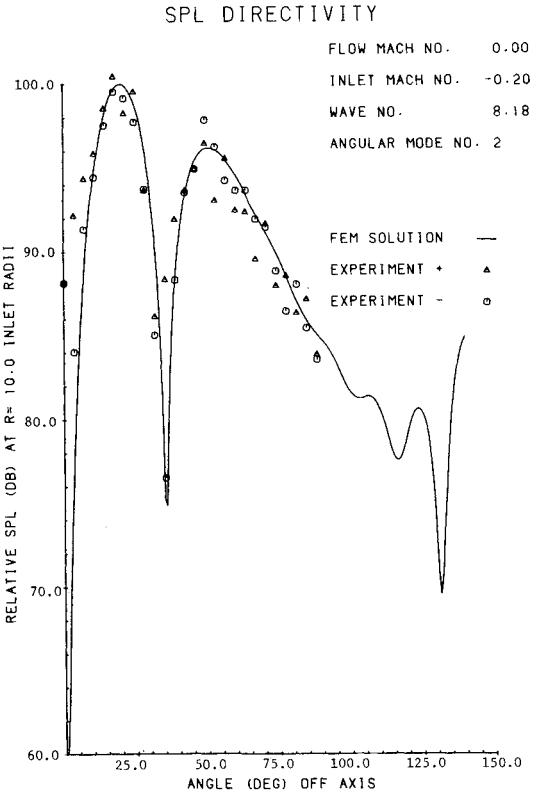

Fig. 6 SPL directivity, bellmouth inlet, $\kappa=8.18$.

axis of symmetry) lobes of equal strength. The L^2 error norm in this case is 0.2% of the analytical solution norm, which is 0.86522.

The results for Mach -0.2 are presented in Figs. 4 and 5. Convective amplification, in which the flow increases the upstream acoustic pressure, is evidenced in the pressure magnitude plot by the upstream (+) lobe being of greater strength than the downstream lobe (the isobars extend further upstream than downstream). The far-field directivities of the numerical and analytical solutions agree closely, however the error norm is 40% of the analytical solution norm, which is 0.88960. A number of factors may contribute to such seemingly poor agreement in the solution norms. First, the analytical solution is linearized to first order in Mach number so that at moderate Mach numbers there is a discrepancy between it and the FE solution. In particular, the constant phase surfaces are different, so phase errors would be expected (the good agreement in the magnitude indicated by the directivity plot would signify that the discrepancy in the norms would be due to phase error). Second, the L^2 error norm would tend to exacerbate phase error effects, since it is effectively the integral of the square of the difference in the two solutions over the domain, and even small phase errors would give large error norms.

Mesh refinement for the Mach -0.2 case gave little change in the directivities and norms. It should be noted that the potential directivity curves are plotted on a logarithmic scale, in a similar manner to SPL directivities.

The results for the juddering sphere agree well with those of Astley.[7] The analytical solutions have been used to validate the FE scheme in terms of flow/acoustic interaction effects; however, the juddering sphere analytical solution comparison is not appropriate at higher Mach numbers, so no further cases are presented.

Inlet Solutions

1) Bellmouth Inlet: A description of the geometry and acoustic spinning mode synthesizer for this test inlet is included in Ref. 11, which also shows the experimental test apparatus. Figures 6 and 7 show the directivity and pressure magnitude plots for the Bellmouth inlet at $\kappa = 8.18$, inlet Mach number of -0.2, and zero external Mach number, for a spinning mode number of 2, with the first 2 radial modes incident. Experimental measurements were taken at a fixed radius from the center of the inlet plane on both sides of the inlet. Since the directivity data obtained are different for either side of the inlet, Fig. 6 shows two sets of results designated + and −. For numerical comparison purposes, the data were averaged and the maximum average designated to be 100 dB. The relative phase between the two modes is set at 30 deg with the second mode leading. Tests with various phase angles showed this to be in good agreement with the experimental results. A range of relatively low frequencies has been studied and the results show very good agreement with the static inlet experimental data. Tests in changing the baffle angle show little evidence of spurious reflections in the peak radiation lobes.

2) Flight Inlet: Numerical calculations were made for a range of frequencies from 3204 to 5645 Hz, corresponding to a wave number range $\kappa = 14.77$-26.25, for no-flow, inflow, and full internal and external flow conditions. Details of the experimental setup and procedures are described in Ref. 12. Wave envelope elements incorporating decay in their interpolation functions were used. A mesh size based on five elements per wavelength for a κ value of 26.25 was used for all the cases, giving 5355 nodes, 1732 elements, and a CPU solution time for the acoustics problem of approximately 18 min on an IBM 4341 computer under the IBM FORTRAN G compiler. The storage required was approximately 1100 kilobytes. The first radial mode is incident and the spinning mode number is 13. The baffle angle used for the mesh was 135 deg, and in each case the peak in the directivity pattern

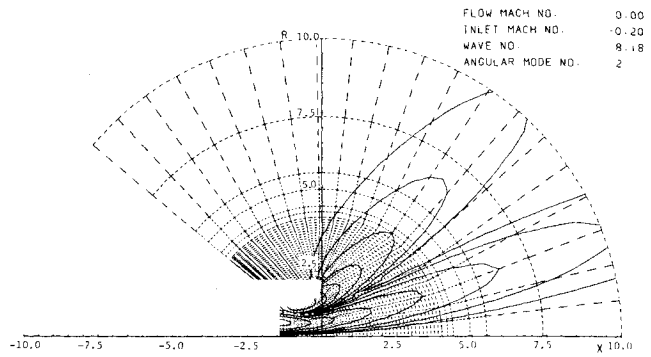

Fig. 7 Pressure magnitude, bellmouth inlet, $\kappa = 8.18$.

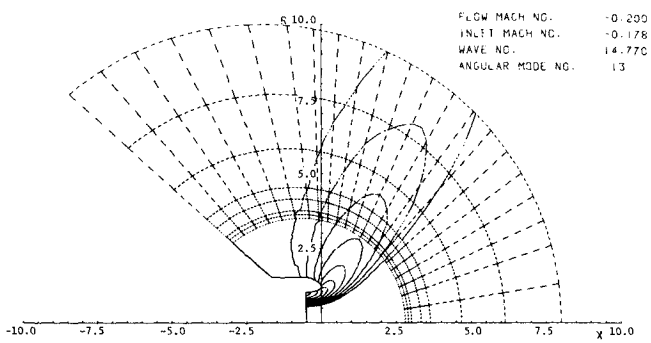

Fig. 8 Pressure magnitude, flight inlet, $\kappa = 14.77$.

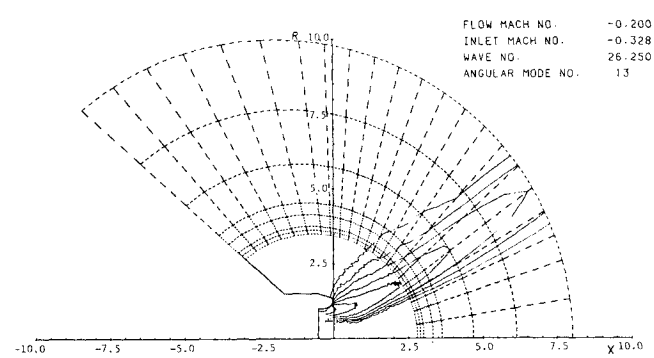

Fig. 9 Pressure magnitude, flight inlet, $\kappa = 26.25$.

was reflection-free. Tests in changing the baffle angle produced little change in the directivity and magnitude plots. Table 1 shows the peak pressure lobe angle for the various wave numbers and flow situations studied.

The trends evident are that as the wave (hence frequency) is increased, the peak radiation lobe moves forward toward the axis and becomes narrower. These are in agreement with experimental observations and analytical modal cutoff predictions.

Overall, the directivities for the flow cases did not appear to be significantly different from those for the no-flow cases; however, larger variations in Mach numbers should produce more discernible changes.

Pressure magnitude plots are shown for the $\kappa = 14.77$ and 26.25 cases, for illustration purposes. In these plots, the finite elements are not plotted, since the mesh is very fine and plotting the elements would obscure the constant pressure contours.

The pressure magnitude contour plot for the wave number $\kappa = 14.77$ under full flow conditions, Fig. 8, shows the peak lobe in relation to the inlet and baffle. There are seven layers

Table 1 Peak radiation lobe angles for JT15D test engine inlet

Wave number[a]	Cutoff ratio[b]	No-flow angle, deg	Inflow		Inflow and external flow	
			Mach no.	Angle, deg	Mach no.	Angle, deg
14.77	0.99	66.3	−0.178	66.5	−0.2	63.8
17.49	1.17	55.0	−0.211		−0.2	54.6
18.81	1.26	50.8	−0.227		−0.2	51.2
20.16	1.35	48.0	−0.238	48.5	−0.2	47.7
20.93	1.40	47.0	−0.254		−0.2	46.0
22.92	1.54	42.3	−0.280		−0.2	41.9
23.59	1.58	40.3	−0.289		−0.2	40.7
26.25	1.76	37.5	−0.328	39.7	−0.2	36.9

[a]Wave number based on no-flow conditions. [b]Cutoff ratio is for the (13,0) mode for no-flow conditions.

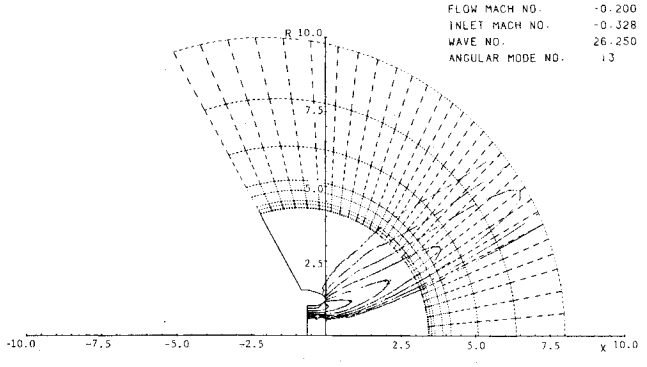

Fig. 10 Pressure magnitude, flight inlet, $\kappa = 26.25$ (refined mesh).

of wave envelope elements, and the contours show a smooth (reflection-free) transition between the finite element and wave enveloped element regions. Numerical experiments indicated that use of wave envelope elements without decay terms in their interpolation functions gave rise to reflections at the transition, extending back into the FE domain. These could be eliminated by increasing the radius of the transition and making a more gradual change in the element sizing in the outer domain. The reason for the reflections is not clear. The envelope functions with decay terms should model point source decay more closely than those without, given that the mesh is constructed on the basis of the monopole solution, which has decay. It is possible that the decay terms "damp" the solution some extent by more closely simulating an outgoing wave and by better modeling the far-field boundary condition, which is also based on the monopole solution. Although the point source assumption may not be entirely valid in this region, the quadratic interpolation functions within the wave envelope element should compensate for some of the discrepancies between the actual and assumed function behavior.

An increase in frequency for a given mesh also gives rise to reflections from the transition region. Figure 9, the full-flow case for a wave number $\kappa = 26.25$, shows evidence of reflections in the FE region, which appear to be more severe near the transition. It has been found that as the wave number is increased, the distance of transition to a point source at the origin approximation should be increased.

The acoustic pressure magnitude plots for the wave number 26.25 obtained with a refined mesh is shown in Fig. 10 for the case with flow. The mesh contained 10201 nodes and 3294 elements. The effect of the mesh refinement is to eliminate oscillations in the contours. The outward shift of the transition radius (cf. Fig. 9) also reduces reflections. The size change in elements away from the transition has been graduated, with the first layer of wave envelope elements less than twice the thickness of the neighboring finite elements. Because of high frequency, the dimension of the finite elements in the (spherically) radial direction is much less than that in the circumferential direction. This can give rise to degradation in the solution accuracy in some circumstances; however, it is more likely that it affects the contour plotting to a much greater degree. Contour oscillations can occur because the plotting method used here relies on linear interpolation of nodal pressures calculated from the potential which has derivatives that are discontinuous across element boundaries. Refinement of the mesh in the circumferential direction alleviates the problem (Fig. 10), but the bandwidths of the resultant matrices become large, and computer solution time increases (the CPU solution time for the 10201 node mesh was 48 min compared with 18 for the 5355 node mesh). Further investigation is required to fully resolve the cause of oscillations and reflections at interfaces such as those encountered here.

The results over the range of frequencies have been presented with the experimental measurements in Ref. 12. The trends evident in the numerical results, as mentioned previously, agree with experimental observations and analytical modal cutoff predictions, however there is a slight discrepancy between the predicted and measured peak radiation angles. It is thought that the flow profile existing in the engine was not uniform across the inlet. If it were not, the inlet acoustic field would not be modeled appropriately by the uniform duct eigenfunctions, so the resultant directivity would not match. The numerical method used has been tested against a variety of known solutions, and mesh refinement, change of baffle angle, and even minor wave number corrections have not produced significant change in the peak radiation directivities.

The computer times given are quoted for an IBM 4341 computer, a relatively slow but inexpensive machine. A reduction factor in CPU time of 5-6 can be obtained on an Amdahl V7 computer under the IBM FORTRAN H (optimized, level 2) compiler.

Conclusions

This project has extended the use of a technique combining finite elements and wave envelope elements, elements that simulate decay and wavelike behavior in their interpolation functions, from the no-flow acoustic radiation problem in which they have been proved to cases incorporating mean flow. The acoustics problem has been posed in an axisymmetric formulation in terms of acoustic velocity potential, to minimize computer solution storage requirements.

A standard finite element approximation is used to solve for the flowfield; then the acoustics problem with flow is solved. The wave envelope mesh geometry is based on the ray paths and constant phase surfaces of the analytical solution for the acoustic field for a monopole in uniform flow. The choice of such a mesh allows simple implementation of a far-field Sommerfeld radiation condition in a manner similar to the no-flow case.

The solution method has been tested and proven against analytical solutions and test engine data.

The modest storage requirements and solution times mean that high wave number problems can be successfully modeled and radiation patterns predicted. Wave numbers as high as 26 have been used, and higher ones are feasible. As the wave number is increased, the distance from the origin at which the transition between finite and wave envelope elements is made should increase to avoid reflections in the solution in the finite element region. Wave envelope elements both with and without decay parameters in their interpolation functions have been used, and it has been found that those with decay terms can alleviate reflection problems to some extent. The thickness of the wave envelope element layers should be gradually increased away from the finite element-wave envelope element transition from a value less than approximately twice the thickness of the adjoining finite element layer. Based on L^2 norm considerations, the finite element mesh resolution was set at a minimum of five elements per acoustic wavelength in the near field. Small-scale geometric and flow effects present in certain problems may require even finer resolution.

Acknowledgment

This work has been carried out under the support of NASA Grant NAG-1-198 from the NASA Langley Research Center.

References

[1]Astley, R. J. and Eversman, W., "A Finite Element Method for Transmission in Non-Uniform Ducts without Flow: Comparison with the Method of Weighted Residuals," *Journal of Sound and Vibration*, Vol. 57, No. 3, 1978, pp. 367-388.

[2]Majjigi, R. K., Sigman, R. K., and Zinn, B. T., "Wave Propagation in Ducts using the Finite Element Method," AIAA Paper 79-0695, 1979.

[3]Tag, I. and Lumsdaine, E., "An Efficient Finite Element Solution for Sound Propagation in Axisymmetric Hard Walled Ducts Carrying High Subsonic Mach Number Flows," AIAA Paper 78-1154, 1978.

[4]Horowitz, S. J., Sigman, R. K., and Zinn, B. T., "An Iterative Finite Element-Integral Technique for Predicting Sound Radiation from Turbofan Inlets in Steady Flight," AIAA Paper 82-0124, 1982.

[5]Horowitz, S. J., Sigman, R. K., and Zinn, B. T., "An Iterative Finite Element-Integral Technique for Predicting Sound Radiation from Turbofan Inlets," AIAA Paper 81-1987, 1981.

[6]Astley, R. J. and Eversman, W., "Finite Element Formulations for Acoustical Radiation," *Journal of Sound and Vibration*, Vol. 88, No. 1, 1983, pp. 47-64.

[7]Astley, R. J., "Acoustical Radiation in Moving Flows: A Finite Element Approach," *Proceedings of the 1983 International Conference on Computational Techniques and Applications*, Sydney, Australia, 1983, pp. 685-698.

[8]Becker, E., Carey, G. F., and Oden, J. T., *Finite Elements: An Introduction*, Prentice-Hall, Inc., Englewood Cliffs, NJ, 1981.

[9]Taylor, K., "Acoustic Generation by Vibrating Bodies in Homentropic Potential Flow at Low Mach Number," *Journal of Sound and Vibration*, Vol. 65, No. 1, 1979, pp. 125-136.

[10]Astley, R. J. and Eversman, W., "A Finite Elment Formulation for the Eigenvalue Problem in Lined Ducts with Flow," *Journal of Sound and Vibration*, Vol. 65, No. 1, 1979, pp. 61-74.

[11]Silcox, R. J., "Experimental Investigation of Geometry and Flow Effects on the Acoustic Radiation from Duct Inlets," AIAA Paper 83-0713, 1983.

[12]Preisser, J. S., Silcox, R. J., Eversman, W., and Parrett, A. V., "A Flight Study of Tone Radiation Patterns Generated by Inlet Rods in a Small Turbofan Engine," AIAA Paper 84-0499, 1984.